Inorganic Chemistry

Article

pubs.acs.org/IC

Cyanomethylene-bis(phosphonate)-Based Lanthanide Complexes: Structural, Photophysical, and Magnetic Investigations**

Catalin Maxim,[†,‡] Diana G. Branzea,[†] Carmen Tiseanu,[§] Mathieu Rouzières,[⊥,¶] Rodolphe Clérac,[⊥,¶] Marius Andruh,[‡] and Narcis Avarvari*[,†]

[†]Laboratoire MOLTECH-Anjou UMR 6200, UFR Sciences, CNRS, Université d'Angers, Bât. K, 2 Bd. Lavoisier, 49045 Angers, France

[‡]Faculty of Chemistry, Inorganic Chemistry Laboratory Str., University of Bucharest, Dumbrava Rosie nr. 23, 020464-Bucharest, Romania

[§]Laboratory of Solid-State Quantum Electronics, National Institute for Laser, Plasma, and Radiation Physics, P.O. Box MG-36, Magurele 077125, Romania

[⊥]CNRS, CRPP, UPR 8641, F-33600 Pessac, France

[¶]University of Bordeaux, CRPP, UPR 8641, F-33600 Pessac, France

Supporting Information

ABSTRACT: The syntheses, structural investigations, magnetic and photophysical properties of a series of 10 lanthanide mononuclear complexes, containing the heteroditopic ligand cyanomethylene-bis(5,5-dimethyl-2-oxo-1,3,2λ^5-dioxa-phosphorinane) (**L**), are described. The crystallographic analyses indicate two structural types: in the first one, $[Ln^{III}(\mathbf{L})_3(H_2O)_2]\cdot H_2O$ (Ln = La, Pr, Nd), the metal ions are eight-coordinated within a square antiprism geometry, while the second one, $[Ln^{III}(\mathbf{L})_3(H_2O)]\cdot 8H_2O$ (Ln = Sm, Eu, Gd, Tb, Dy, Ho, Er), contains seven-coordinated Ln^{III} ions within distorted monocapped trigonal prisms. Intermolecular hydrogen bonding between nitrogen atoms of the cyano groups, crystallization, and coordination water molecules leads to the formation of extended supramolecular networks. Solid-state photophysical investigations demonstrate that Eu^{III} and Tb^{III} complexes possess intense luminescence with relatively long excited-state lifetimes of 530 and 1370 μs, respectively, while Pr^{III}, Dy^{III}, and Ho^{III} complexes have weak intensity luminescence characterized by short lifetimes ranging between a few nanoseconds to microseconds. The magnetic properties for Pr^{III}, Gd^{III}, Tb^{III}, Dy^{III}, and Ho^{III} complexes are in agreement with isolated Ln^{III} ions in the solid state, as suggested by the single-crystal X-ray analyses. Alternating current (ac) susceptibility measurements up to 10 kHz reveal that only the Ho^{III} complex shows a frequency-dependent ac response, with a relaxation mode clearly observed at 1.85 K around 4500 Hz.

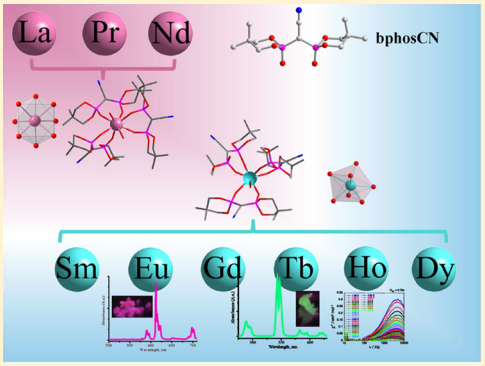

INTRODUCTION

Functionalized acetylacetonate (acac) ligands such as 3-(4-pyridyl)-acetylacetonate (acacPy)[1] and 3-cyano-acetylacetonate (acacCN)[2] have emerged in the past decade as useful ditopical ligands combining one hard *O*,*O*-chelating site with one *N* donor site, which can in principle act either as ligand toward a second metal center or as hydrogen bond acceptor.

In this respect, the acacCN ligand provided monometallic Co(II),[3] Zn(II),[4] or Cu(II)[2,5] transition-metal complexes, together with heterometallic Cu(II)−Ag(I),[6] Fe(III)−Ag(I),[6] Al(III)−Ag(I),[6,7] or Cr(III)−Ag(I)[8] coordination polymers. Heteroleptic extended networks Cu(II)−Ag(I) and Co(III)−Ag(I) have also been obtained by combining acacCN and dipyrrin (dpm) ligands.[9] Interestingly, the homoleptic complexes $Al(acacCN)_3$ and $Cr(acacCN)_3$ have been investigated as sensitizers for lanthanide-centered luminescence through the preparation and photophysical properties of a series of bimetallic 2d/3d−4f complexes formulated as $[(acacCN)_2M(\mu\text{-acacCN})LnCl_3]$ (M = Al, Cr; Ln = Sm, Eu, Tb, Yb).[10] It is assumed in these complexes that the lanthanide ions are coordinated by one of the cyano groups of the acacCN ligands. However, the acacCN ligand is particularly well-suited to coordinate Ln centers through the *O*,*O*-chelating motif, as recently demonstrated by Englert et al. who described a series of $Ln(acacCN)_3$ (Ln = Ce, Eu, Yb) complexes together with their extended heterometallic $Ln(acacCN)_4Ag$ networks.[11] The interest in lanthanide-based complexes resides on the one hand on their peculiar photophysical properties, as they generally have long excited-state lifetimes,[12] making them very attractive for applications such as fluorescent displays, electroluminescent devices, biomedical imaging, etc.[13] On the other hand, in the field of molecular magnetism the main recent interest is directed toward the use of highly anisotropic Ln ions, such as

Received: December 19, 2013
Published: February 20, 2014

   dx.doi.org/10.1021/ic403104y | *Inorg. Chem.* 2014, 53, 2708−2717

Tb(III), Dy(III), or Ho(III), to synthesize single-molecule magnets (SMM)[14,15] and single-chain magnets (SCM).[16]

We have recently introduced in the coordination chemistry area phosphorus analogues of the acacCN ligand, namely, the cyanomethylene-bis(5,5-dimethyl-2-oxo-1,3,2λ^5-dioxa-phosphorinane) anionic derivative **L** (or bphosCN, Scheme 1),

Scheme 1. Functional Acetylacetonate and Bis(phosphonate) Ligands

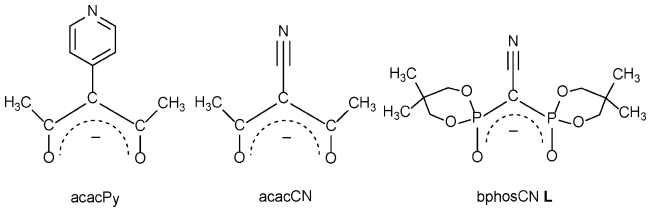

containing two phosphonate groups. Accordingly, mononuclear Fe(**L**)$_3$ complexes together with a heterometallic Fe(III)−Ag(I) extended coordination network have been described.[17] The advantages of this family of ligands are their modularity, since in principle it is possible to vary the substituents at the phosphorus atoms, their easy characterization by ^{31}P NMR, and their robustness to electrophilic attacks.[18] As their acacCN analogues, they seem particularly well-adapted for lanthanides coordination. We have thus decided to synthesize Ln(III) complexes based on the bphosCN ligand and to investigate their solid-state structures and their photophysical and magnetic properties, especially in the case of the most anisotropic ions for the latter.

RESULTS AND DISCUSSION

Synthesis and Solid-State Structures. A series of 10 lanthanide complexes was synthesized by the direct reaction of Ln(NO$_3$)$_3$ (Ln = La, Pr, Nd, Sm, Eu, Gd, Tb, Dy, Ho, and Er) precursors and the ligand **L** in ethanol. All are discrete mononuclear complexes, and their structures have been confirmed by single-crystal X-ray diffraction studies on crystals obtained by recrystallization in water. The cell determination studies indicate two structural types, that are, type I for the compounds **1**−**3** ([Ln(**L**)$_3$(H$_2$O)$_2$]·H$_2$O; Ln = La, **1**; Pr, **2**; Nd, **3**) and type II for the compounds **4**−**10** ([Ln(**L**)$_3$(H$_2$O)]·8H$_2$O; Ln = Sm, **4**; Eu, **5**; Gd, **6**; Tb, **7**; Dy, **8**; Ho, **9**; Er, **10**), which follow the position of the lanthanide ions in the 4f series.

The compounds **1**−**3**, belonging to type I, have the general formula of [Ln^{III}(**L**)$_3$(H$_2$O)$_2$]·H$_2$O (Ln^{III} = La, **1**; Pr, **2**; Nd, **3**) and crystallize in the chiral $P2_12_12_1$ orthorhombic space group. As an example, the structure of the praseodymium derivative **2** is described in detail. The asymmetric unit consists of one Pr center coordinated by three nonequivalent ligands **L** and two water molecules within a square antiprism geometry, as well as one crystallization water molecule (Figure 1a).

The praseodymium ion is coordinated by eight oxygen atoms forming a distorted triangular dodecahedron or square antiprism (Figure 1b). Six of the oxygen atoms belong to ligand groups (Pr1−O2C = 2.356(2), Pr1−O2A = 2.369(3), Pr1−O1B = 2.437(2), Pr1−O1C = 2.436(2), Pr1−O2B = 2.454(2), Pr1−O1A = 2.500(2) Å), and two belong to water molecules (Pr1−O2 = 2.504(2); Pr1−O1 = 2.575(2) Å). Selected bond lengths and angles involving the lanthanide ion are gathered in Table 1.

At the supramolecular level the mononuclear entities interact through hydrogen bonds established between the nitrogen (N1A) atom of one ligand groups and the aqua ligand (O2) belonging to a neighboring unit, thus affording supramolecular zigzag chains (Figure 2). The other coordinated water molecule (O1) forms a hydrogen bond [O1−O1w = 2.74 Å] with the crystallization water molecule (O1w).

The shortest Pr···Pr distances measured within a chain amount to 11.63 Å, while longer distances of 12.17 Å are observed between Pr centers belonging to parallel chains (Figure 3). These intermolecular distances are long enough to prevent any significant magnetic interactions between the lanthanide ions.

The infrared (IR) spectrum of complex **2** (Supporting Information, Figure S1) is dominated by the presence of the characteristic bands of the bphosCN ligand, with the absorption of the CN group at 2180 cm^{-1} and that of the P═O groups at 1220 cm^{-1}.

The complexes **4**−**10**, belonging to type II system, [Ln^{III}(**L**)$_3$(H$_2$O)]·8H$_2$O (Ln^{III} = Sm, **4**; Eu, **5**; Gd, **6**; Tb, **7**; Dy, **8**; Ho, **9**; Er, **10**) are isostructural and crystallize in the noncentrosymmetric monoclinic space group *Pn*. Here, the crystal structure of the Tb(III) analogue is described as an example for this series of complexes (Figure 4). The asymmetric unit consists of a mononuclear complex and eight

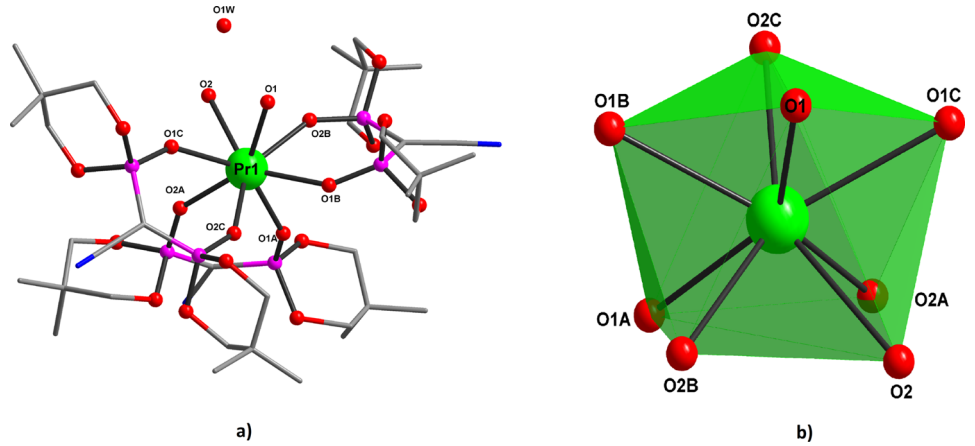

Figure 1. (a) Molecular structure of **2** in the solid state (H atoms are omitted for clarity). (b) Local coordination geometry of the Pr(III) ion in **2**.

dx.doi.org/10.1021/ic403104y | *Inorg. Chem.* 2014, 53, 2708−2717

Table 1. Selected Bond Lengths (Å) and Angles (deg) for Compounds 1−10

1	2	3	4	5
La1 O2C 2.398(3)	Pr1 O2C 2.356(2)	Nd O2C 2.340(3)	Sm O1A 2.308(3)	Eu1 O1A 2.311(4)
La1 O2A 2.413(3)	Pr1 O2A 2.369(3)	Nd O2A 2.362(3)	Sm O1B 2.322(3)	Eu1 O1B 2.313(3)
La1 O1B 2.471(2)	Pr1 O1B 2.437(2)	Nd O1B 2.425(3)	Sm O1C 2.348(3)	Eu1 O1C 2.343(3)
La1 O1C 2.476(2)	Pr1 O1C 2.436(2)	Nd O1C 2.426(3)	Sm O3B 2.358(4)	Eu1 O2A 2.348(4)
La1 O2B 2.495(2)	Pr1 O2B 2.454(2)	Nd O2B 2.442(3)	Sm O2A 2.361(4)	Eu1 O3B 2.361(4)
La1 O1A 2.544(2)	Pr1 O1A 2.500(2)	Nd O2 2.483(3)	Sm O1E 2.375(3)	Eu1 O1E 2.370(3)
La1 O2 2.557(3)	Pr1 O2 2.504(3)	Nd O1A 2.494(3)	Sm O1 2.385(3)	Eu1 O1 2.384(3)
La1 O1 2.616(2)	Pr1 O1 2.575(2)	Nd O1 2.554(3)	O1A Sm O1B 92.99(18)	O1A Eu1 O1B 92.81(17)
O2C La1 O2A 85.11(12)	O2C Pr1 O2A 84.77(12)	O2C Nd O2A 84.52(14)	O1A Sm O1C 84.01(17)	O1A Eu1 O1C 83.93(16)
O2C La1 O1B 74.29(9)	O2C Pr1 O1B 74.35(9)	O2C Nd O1B 74.32(11)	O1B Sm O1C 175.06(14)	O1B Eu1 O1C 174.59(13)
O2A La1 O1B 141.37(10)	O2A Pr1 O1B 142.58(10)	O2A Nd O1B 142.17(11)	O1A Sm O3B 76.62(15)	O1A Eu1 O2A 73.62(13)
O2C La1 O1C 72.44(8)	O2C Pr1 O1C 73.20(8)	O2C Nd O1C 73.60(10)	O1B Sm O3B 74.67(12)	O1B Eu1 O2A 84.81(14)
O2A La1 O1C 75.14(9)	O2A Pr1 O1C 75.33(9)	O2A Nd O1C 75.48(11)	O1C Sm O3B 108.31(13)	O1C Eu1 O2A 90.13(14)
O1B La1 O1C 126.18(9)	O1B Pr1 O1C 125.13(9)	O1B Nd O1C 125.40(10)	O1A Sm O2A 73.06(13)	O1A Eu1 O3B 76.61(15)
O2C La1 O2B 144.67(9)	O2C Pr1 O2B 145.22(9)	O2C Nd O2B 145.51(11)	O1B Sm O2A 85.14(15)	O1B Eu1 O3B 75.02(12)
O2A La1 O2B 119.83(10)	O2A Pr1 O2B 119.33(11)	O2A Nd O2B 119.41(12)	O1C Sm O2A 90.23(14)	O1C Eu1 O3B 108.26(13)
O1B La1 O2B 70.80(8)	O1B Pr1 O2B 71.56(8)	O1B Nd O2B 71.83(10)	O3B Sm O2A 142.38(12)	O2A Eu1 O3B 142.92(12)
O1C La1 O2B 134.73(8)	O1C Pr1 O2B 133.98(8)	O1C Nd O2B 133.31(10)	O1A Sm O1E 135.79(13)	O1A Eu1 O1E 136.04(14)
6	**7**	**8**	**9**	**10**
Gd O1B 2.298(3)	Tb O1A 2.278(4)	Dy O1B 2.270(4)	Ho O1A 2.258(4)	Er1 O1A 2.240(10)
Gd O1A 2.300(4)	Tb O1B 2.296(4)	Dy O1A 2.276(4)	Ho O1B 2.270(3)	Er1 O1C 2.242(8)
Gd O1C 2.330(3)	Tb O1C 2.304(4)	Dy O1C 2.296(4)	Ho O1C 2.279(3)	Er1 O1B 2.246(8)
Gd O2A 2.336(4)	Tb O2A 2.305(5)	Dy O2A 2.310(5)	Ho O2A 2.295(4)	Er1 O1E 2.278(8)
Gd O3B 2.350(4)	Tb O1E 2.333(3)	Dy O3B 2.322(5)	Ho O3B 2.311(4)	Er1 O2A 2.293(9)
Gd O1E 2.363(3)	Tb O3B 2.345(5)	Dy O1 2.327(4)	Ho O1E 2.312(3)	Er1 O3B 2.315(11)
Gd O1 2.367(3)	Tb O1 2.356(4)	Dy O1E 2.330(4)	Ho O1 2.319(3)	Er1 O1 2.324(8)
O1B Gd O1A 93.01(16)	O1A Tb O1B 92.40(18)	O1B Dy O1A 92.6(2)	O1A Ho O1B 92.78(17)	O1A Er1 O1C 83.9(4)
O1B Gd O1C 174.57(14)	O1A Tb O1C 83.68(18)	O1B Dy O1C 174.05(15)	O1A Ho O1C 83.65(16)	O1A Er1 O1B 92.2(4)
O1A Gd O1C 83.66(16)	O1B Tb O1C 174.24(16)	O1A Dy O1C 83.76(19)	O1B Ho O1C 174.18(13)	O1C Er1 O1B 173.8(3)
O1B Gd O2A 85.20(15)	O1A Tb O2A 73.77(18)	O1B Dy O2A 85.11(17)	O1A Ho O2A 74.26(14)	O1A Er1 O1E 136.7(3)
O1A Gd O2A 73.64(15)	O1B Tb O2A 85.42(19)	O1A Dy O2A 74.06(17)	O1B Ho O2A 85.54(15)	O1C Er1 O1E 75.8(3)
O1C Gd O2A 89.74(14)	O1C Tb O2A 89.42(19)	O1C Dy O2A 89.37(17)	O1C Ho O2A 89.06(15)	O1B Er1 O1E 110.3(3)
O1B Gd O3B 75.48(13)	O1A Tb O1E 136.39(15)	O1B Dy O3B 76.19(16)	O1A Ho O3B 76.44(15)	O1A Er1 O2A 74.5(4)
O1A Gd O3B 76.24(15)	O1B Tb O1E 110.73(14)	O1A Dy O3B 76.24(18)	O1B Ho O3B 76.28(13)	O1C Er1 O2A 89.2(4)
O1C Gd O3B 107.74(13)	O1C Tb O1E 74.96(14)	O1C Dy O3B 107.34(17)	O1C Ho O3B 107.20(13)	O1B Er1 O2A 85.2(4)

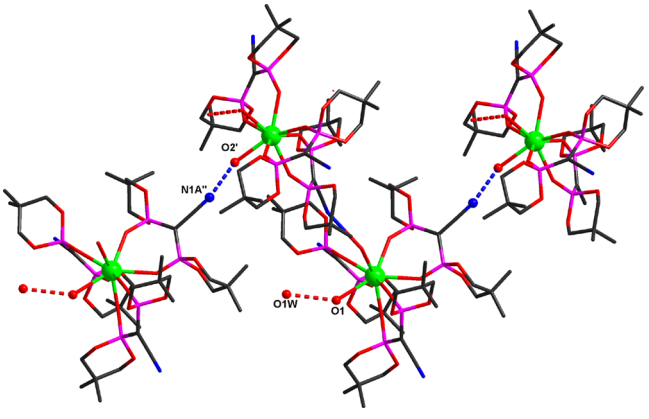

Figure 2. Formation of supramolecular chains in complex **2**, with the shortest N···O contacts highlighted in dotted blue lines (′ = −*x*, −0.5 + *y*, 0.5 − *z*; ″ = −1 + *x*, −1 + *y*, −1 + *z*).

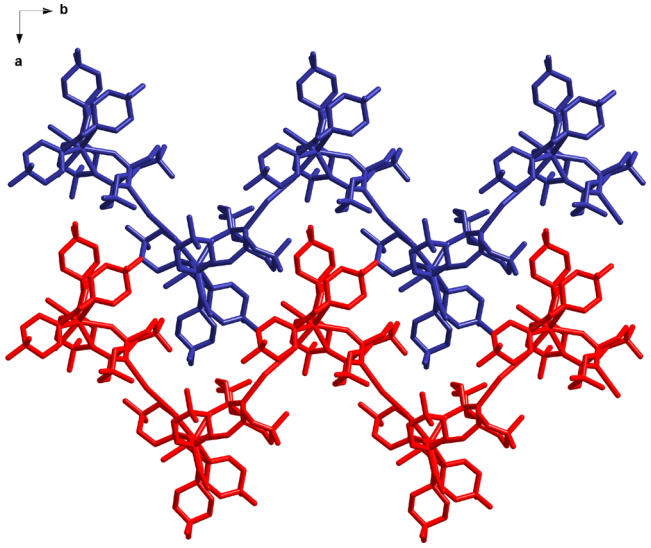

Figure 3. Successive parallel chains in the (*a*,*b*) plane of the crystal structure of complex **2**.

noncoordinated water molecules in general positions. The coordination geometry of the Tb(III) ion can be described as a distorted monocapped trigonal prism (Figure 4), with the O1A atom at the corner of the prism, and the O1C, O3B, O1E, O1B, O2A, and O1 atoms forming the basal triangular planes of the polyhedron. The distances from the Tb(III) site to the two triangular planes are particularly short at 1.357 and 1.489 Å. The Ln−O bond lengths range from 2.308(3) to 2.385(3) Å

dx.doi.org/10.1021/ic403104y | *Inorg. Chem.* 2014, 53, 2708−2717

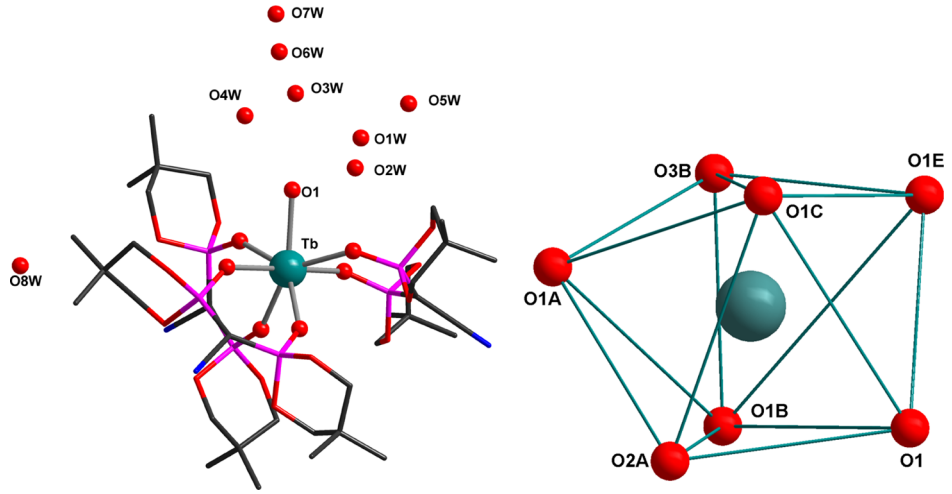

Figure 4. (left) Perspective view of the asymmetric unit of complex **7** (H atoms are omitted for clarity). (right) Local coordination geometry of the Tb(III) ion in complex **7**.

for complex **4**, 2.311(4) to 2.384(3) Å for **5**, 2.298(3) to 2.367(3) Å for **6**, 2.278(4) to 2.356(4) Å for **7**, 2.270(4) to 2.330(4) Å for **8**, 2.258(4) to 2.319(3) Å for **9**, and 2.240(10) to 2.324(8) Å for **10**.

In the packing diagram shown in Figure 5, the mononuclear species are interconnected into a complex network through

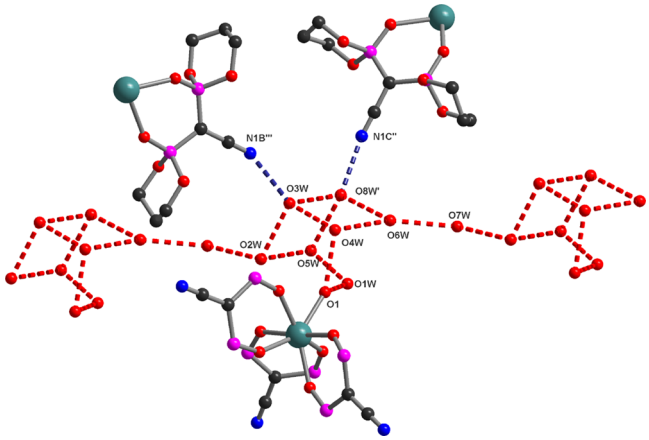

Figure 5. A portion of the structure highlighting the one-dimensional hydrogen bonding network formed by the alternating octameric water clusters in complex **7** (′ = x, 1 + y, z; ″ = 0.5 + x, 1 − y, 0.5 + z, ‴ = −0.5 + x, 1 − y, 0.5 + z).

hydrogen bonds established between the lattice water molecules, the aqua ligands, and the nitrogen atoms of the cyano groups of the chelating bisphosphonate ligand. An interesting feature of this crystal structure is observed looking at the crystallization water molecules, which form octameric clusters with a distorted cubique topology. This arrangement was the first crystallographically characterized organization described for an octameric water cluster.[19] More recently, some of us have described a crown-like octameric water cluster with a D_{4d} symmetry and a bicyclo[2,2,2]octane-like structure.[20]

The distances between the water molecules within the octameric cluster in **7** are in the 2.633−3.064 Å range. These water octamers are further connected to another crystallization water molecule (O6w−O7w = 2.923 Å), thus resulting in one-dimensional water chains running along the a axis (Figure 6).

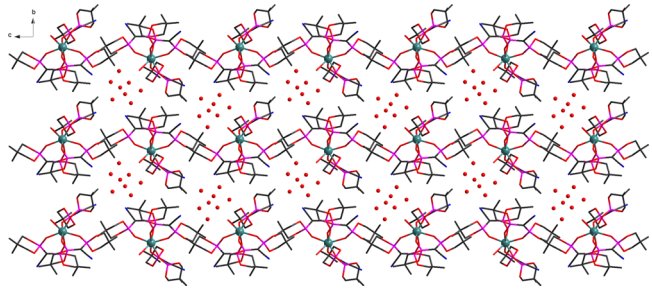

Figure 6. Packing diagram of complex **7** highlighting the water chains running along the a axis.

The shortest Ln···Ln distances in the crystal structures amount to 11.132 Å for complex **4**, 11.885 Å for **5**, 11.881 Å for **6**, 11.838 Å for **7**, 11.131 Å for **8**, 11.139 Å for **9**, and 11.138 Å for **10**. As a consequence, magnetic couplings between the metallic ions are expected to be negligible.

Photophysical Properties. The photophysical properties were determined for the complexes **2** (Pr), **4** (Sm), **5** (Eu), **7** (Tb), **8** (Dy), and **9** (Ho). Figure 7 illustrates the emission spectrum of complex **2** upon excitation at λ_{ex} = 447.4 nm, corresponding to the $^3H_4$−$^3P_2$ absorption of the Pr^{III} ion. The emission includes the superposition from both shorter-lived $^3P_0$ and longer-lived $^1D_2$ levels, based on the evolution of the emission with delay time after the laser pulse. Thus, at a shorter delay of 15 ns, the observed emission lines at 488, 524, 610, 638, 677, 693, and 721 nm can be assigned to $^3P_0$ to $^3H_{4,5,6}$, $^3F_{2,3,4}$ transitions. Increasing the delay to ∼30 ns, the shorter-lived $^3P_0$-related emission is no longer detected, while the remaining emission peaked at 602 nm is assigned to $^1D_2$−$^3H_4$ transition. According to X-ray diffraction data, the Pr^{3+} site is coordinated by three nonequivalent **L** ligands and two water molecules within a square antiprism geometry, one crystallization water molecule being observed as well.

On the other side, the $^1D_2$ and $^3P_0$ levels have an energy gap to the next lower lying level close to ∼6.500 cm^{-1} (relative to $^1G_4$ level) and ∼3.500 cm^{-1} (relative to $^1D_2$ level), respectively, which lead to very efficient nonradiative quenching of the Pr^{III} emission due to coordinated water molecules. In consequence, the emission is weak and short-lived, with lifetimes on the nanosecond scale (Table 2).

dx.doi.org/10.1021/ic403104y | Inorg. Chem. 2014, 53, 2708−2717

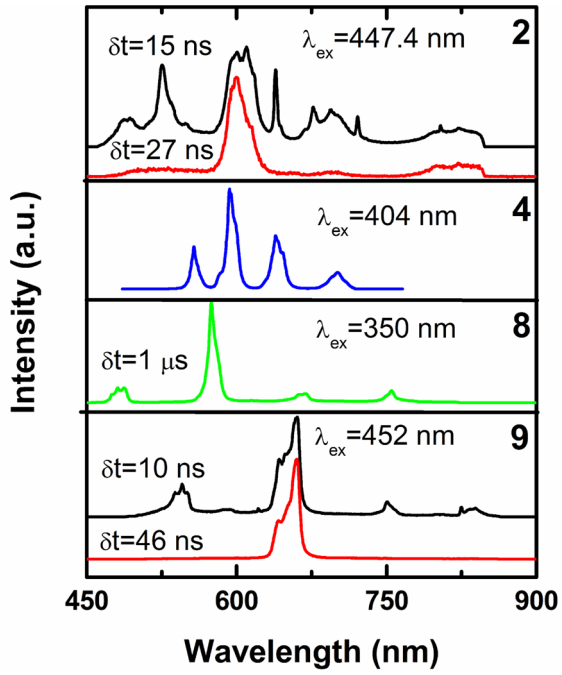

Figure 7. Emission spectra of complexes **2**, **4**, **8**, and **9**. To discriminate among the distinct emitting levels, two delays were used after the laser pulse for complexes **2** and **9**.

Table 2. Emission Lifetimes for Complexes 2, 4, 5, 7, 8, and 9

	short-lived emitting level	long-lived emitting level
Pr^{III}	$^3P_0$ ≈ few ns, below our instrumental resolution of 30 ns	$^1D_2$ few ns, below our instrumental resolution of 30 ns
Sm^{III}	$^4G_{5/2}$ ≈ 6 μs	
Eu^{III}	$^5D_1$ 10 ± 0.15 μs	$^5D_0$ 530 ± 0.015 μs
Tb^{III}	$^5D_4$ 1370 ± 0.0025 μs	
Dy^{III}	$^4F_{9/2}$ 14 μs	
Ho^{III}	$^5S_2$+$^5F_4$ 2.2 μs	$^5F_5$ 16.3 μs

Figure 7 illustrates the emission spectrum of complex **4** excited at λ_{ex} = 404 nm, corresponding to the $^6H_{5/2}$–$^6P_{3/2}$+$^6P_{5/2}$ transitions. The orange-red luminescence centered at ∼556, 594, 639, and 701 nm is assigned to the Sm^{III} $^4G_{5/2}$–$^6H_{5/2}$, $^4G_{5/2}$–$^6H_{7/2}$, $^4G_{5/2}$–$^6H_{9/2}$, and $^4G_{5/2}$–$^6H_{11/2}$ transitions, respectively. The $^4G_{5/2}$–$^6H_{5/2}$ of the Sm^{III} ion has a predominantly magnetic dipole character, whereas the $^4G_{5/2}$–$^6H_{9/2}$ one is predominantly an electric dipole transition with hypersensitivity property (ΔJ = 2). The intensity ratio $I(^4G_{5/2}$–$^6H_{9/2})/I(^4G_{5/2}$–$^6H_{5/2})$ is indicative of departure from centrosymmetry, as the ratio tends to 0 for Sm^{III} ions in centrosymmetric sites.[21] The value close to 2 confirms the low symmetry of the Sm^{III} coordination polyhedron established with the X-ray diffraction analysis. The luminescence decay measured at λ_{ex} = 404 nm and λ_{em} = 594 nm follows a single exponential law with a lifetime of ∼6 μs (Table 2).

Figure 8 gathers the photophysical properties of complex **5**. The excitation spectrum corresponding to λ_{em} = 611.5 nm displays only the f–f absorptions of the Eu^{III} ion, with the most intense ones at 393 and 464 nm (corresponding to the $^7F_0$–$^5L_6$ and $^7F_0$–$^5D_2$ transitions, respectively). The emission spectrum excited at λ_{ex} = 393 nm displays the characteristic Eu^{III}

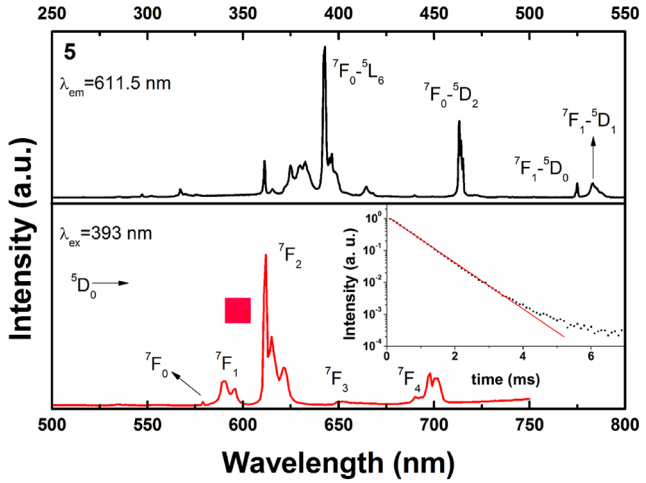

Figure 8. (top) Excitation and (bottom) emission spectrum of complex **5**. Inset represents the emission decay measured with λ_{ex} = 393 nm and λ_{em} = 611.5 nm. The red line represents the result of a monoexponential fitting.

transitions centered at λ_{em} = 579 nm ($^5D_0$–$^7F_0$), 590 nm ($^5D_0$–$^7F_1$), 611.5 nm ($^5D_0$–$^7F_2$), 650 nm ($^5D_0$–$^7F_3$), and 697 nm ($^5D_0$–$^7F_4$). The red emission is quite intense, being observed by naked eyes under standard lamp excitation. Moreover, the emission intensities of **5** and commercial Eu–Y_2O_3 phosphor (K63/UF-P1 from Phosphor Technology) are found to be comparable (see Supporting Information, Figure S2) for an excitation wavelength of 393 nm. Though such comparison is not reliable, it evaluates reasonably the potential phosphor applications of **5**. The intense emission of **5** contrasts with the relatively weak emission of Eu^{III} in complexes with Schiff base ligands, not having a sensitizing effect.[22] Some weak emission related to the upper excited $^5D_1$ is also detected in the spectral range of ∼520–560 nm (Supporting Information, Figure S3). The $^5D_0$–$^7F_1$ emission transition displays three lines (at 589.7, 590.8, and 595.9 nm), which means that the local symmetry at the Eu^{III} sites is C_{2v} or lower (Supporting Information, Figure S4a). Furthermore, the nondegenerate $^5D_0$–$^7F_0$ emission transition is structure less, indicating a single Eu^{III} site in **5** (Supporting Information, Figure S4b). Within the limits of spectral resolution (∼0.01 nm), the $^5D_0$–$^7F_0$ emission line is reasonably fitted with a single Gaussian law with a full width at half-maximum (fwhm) value of ∼0.5 nm. The $^5D_0$–$^7F_2$ transition is of electric dipole nature with hypersensitivity property (ΔJ = 2). The value of four, for the intensity ratio $R = I(^5D_0$–$^7F_2)/I(^5D_0$–$^7F_1)$, known as asymmetry ratio, is indicative of the asymmetry of the coordination polyhedron of the Eu^{III} ion.[23] The luminescence decays measured at λ_{em} = 611.5 nm (corresponding to the $^5D_0$–$^7F_2$ transition) and 535 nm (corresponding to the $^5D_1$–$^7F_1$) for excitation at λ_{ex} = 393 nm can be reasonably fitted with a single exponential law with lifetimes τ of 530 ± 0.015 (Figure 8) and 10 μs ± 0.15 μs, respectively (Table 2). Overall, the shapes of the $^5D_0$-related emission together with its single exponential decay suggest a unique low-symmetry coordination polyhedron for the Eu^{III} site in **5**, a result which can be extended to other Ln^{III} ions in the isostructural **4**, **7**, **8**, and **9** complexes.

Figure 9 gathers the photophysical properties of complex **7**. The excitation spectrum corresponding to λ_{em} = 543 nm consists of several sharp peaks at 284, 294, 302, 317,336, 340, 350, 356, 370, and 376 nm assigned to f–f absorptions of the

dx.doi.org/10.1021/ic403104y | Inorg. Chem. 2014, 53, 2708–2717

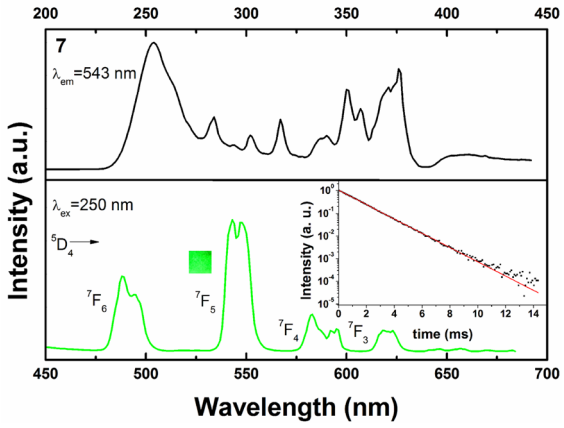

Figure 9. (top) Excitation and (bottom) emission spectrum of complex **7**. Inset represents the emission decay measured λ_{ex} = 250 nm and λ_{em} = 543 nm. The red line represents the result of a monoexponential fitting.

Tb^{III} ion. A relatively strong and broad band centered at 254 nm is assigned to 4f−5d transition,[24] which matches with the emission maximum of commercial Hg lamps. The emission spectrum displays the relatively strong terbium $^5D_4$−^7F_J transitions at 492, 544, 585, and 623 nm for J = 6, 5, 4, and 3, respectively. The emission is dominated by the $^5D_4$−$^7F_5$ transition at 543 nm that exhibits a crystal-field splitting structure. The green emission is strong, being observed by naked eyes under standard lamp excitation. The PL decays measured at λ_{em} = 543 can be reasonably fitted with a single exponential law with a lifetime τ = 1.37 ± 0.0025 ms (Table 2). The lifetime of complex **7** exceeds well the values measured for Tb^{III} in complexes with Schiff-base ligands, which varied between ∼50 and 250 μs.[22b,25]

Figure 7 illustrates the emission spectrum of the Dy complex **8**, excited at 350 nm, corresponding to $^6H_{15/2}$−$P_{7/2}$ transition. The characteristic emissions of the Dy^{III} ion are revealed at 482, 574, 665, and 754 nm, corresponding to $^4F_{9/2}$−$^6H_{15/2}$, $^4F_{9/2}$−$^6H_{13/2}$, $^4F_{9/2}$−$^6H_{11//2}$, and $^4F_{9/2}$−$^6H_{9/2}$/$^6F_{11/2}$ transitions, respectively. The emission decay measured at λ_{em} = 574 nm shows an exponential variation, with a lifetime of ∼14 μs (Table 2). Finally, Figure 7 illustrates the emission spectrum of the Ho^{III} ion in complex **9** excited at 452 nm, which corresponds to the $^5I_8$−$^5G_6$ absorption transition. The emissions at 544, 660, and 751 nm are assigned to $^5S_2$+$^5F_4$−$^5I_8$, $^5F_5$−$^5I_8$, and $^5S_2$+$^5F_4$−$^5I_7$, and $^5S_2$+$^5F_4$−$^5I_5$ transitions, respectively. The emission related to longer-lived $^5F_5$ level is discriminated by use of a delay of 45 ns. The emission lifetimes corresponding to $^5S_2$+$^5F_4$ (λ_{em} = 544 nm) and $^5F_5$ (λ_{em} = 660 nm) are short, being estimated at around 2.2 and 16.3 μs, respectively (Table 2).

To summarize, complexes **5** and **7** display a bright luminescence with relatively long lifetimes of 530 and 1370 μs, respectively. In contrast, the emissions of **2**, **8**, and **9** have weak intensity with short lifetimes varying from few nanoseconds (**2**) to few microseconds (**8** and **9**).

Magnetic Properties. The magnetic properties of the complexes **2** (Pr), **6** (Gd), **7** (Tb), **8** (Dy), and **9** (Ho) were studied using combined dc and ac magnetic measurements. The room-temperature values of the χT product for the mononuclear complexes **2** and **6**−**9** are presented in Table 3. For these compounds, which contain Ln^{III} ions with a good energetic separation between the ground state and the first excited state, the magnetic susceptibility is easily calculated using the following relation: $\chi = (Ng_J^2\mu_B^2/3k_BT)J(J+1)$, where $g_J = 3/2 + [S(S+1) - L(L+1)]/2J(J+1)$.[26] The theoretical and experimental values are in excellent agreement for the five measured compounds.

For the gadolinium derivative **6**, the magnetic data follow perfectly the expected $\chi T = C = 21N\mu_B^2/k_B$ Curie law (Figure 10). Decreasing the temperature, the χT product remains

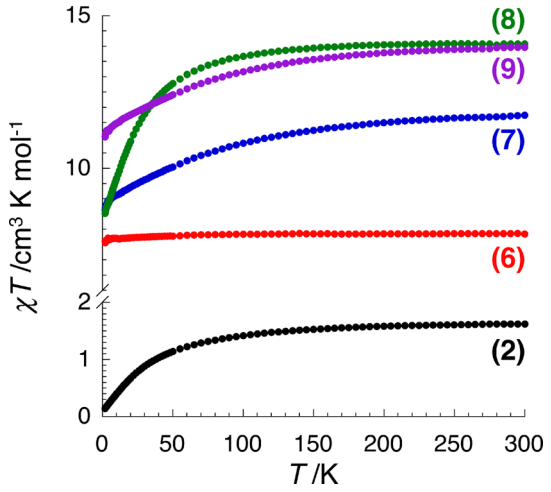

Figure 10. Temperature dependence of the χT product for complexes **2** and **6**−**9** at 1000 Oe (with χ defined as molar magnetic susceptibility equal to M/H per mole of mononuclear complex).

constant to 1.8 K, indicating the absence of any significant magnetic interaction between mononuclear Gd^{III} species in the solid state. For the other complexes, the χT product decreases continuously as the temperature is lowered due to the well-known thermal depopulation of the Stark levels (Figure 10).[27]

The field dependence of the magnetization was also measured for these five complexes. While the Pr analogue displays a linear and weak dependence of the magnetization (Supporting Information, Figure S5) expected for a weakly magnetic system (0.4 μ_B at 1.85 K and 7 T), the paramagnetic Gd complex reaches 7.3 μ_B at 1.85 K and 7 T (Supporting Information, Figure S6), expected for S = 7/2 species. In the cases of **7**, **8**, and **9**, the magnetization at 1.85 or 2 K does not

Table 3. Theoretical and Experimental Room-Temperature Values of the χT Product for Complexes 2 and 6−9

compound	formula	S	L	g_J	$(\chi T)_{theo}$ (cm^3 K/mol)	$(\chi T)_{exp}$ (cm^3 K/mol)
2 Pr^{III}	$[Pr^{III}(bphosCN)_3(H_2O)_2]\cdot H_2O$	1	5	4/5	1.60	1.6
6 Gd^{III}	$[Gd^{III}(bphosCN)_3(H_2O)]\cdot 8H_2O$	7/2	0	2	7.875	7.9
7 Tb^{III}	$[Tb^{III}(bphosCN)_3(H_2O)]\cdot 8H_2O$	3	3	3/2	11.8125	11.8
8 Dy^{III}	$[Dy^{III}(bphosCN)_3(H_2O)]\cdot 8H_2O$	5/2	5	4/3	14.166	14.1
9 Ho^{III}	$[Ho^{III}(bphosCN)_3(H_2O)]\cdot 8H_2O$	2	6	5/4	14.063	14.0

dx.doi.org/10.1021/ic403104y | Inorg. Chem. 2014, 53, 2708−2717

saturate even at 7 T, reaching 4.9, 6.1, and 5.6 μ_B, respectively (Supporting Information, Figures S7–S9). The high-field linear behavior of the magnetization indicates a significant amount of magnetic anisotropy in these complexes as expected for the trivalent terbium, dysprosium, and holmium ions that are usually characterized by a strong magnetic anisotropy, frequently employed to obtain single-molecule magnet or single-chain magnet systems. Consequently, the dynamic magnetic properties of compounds **7**–**9** were investigated using dc and ac susceptibility measurements. With traditional field sweeping rates of our commercial SQUID magnetometer, none of the complexes display *M* versus *H* hysteresis effect above 1.85 K and thus slow relaxation of the magnetization. The investigation of shorter time scale, using ac susceptibility measurements up to 10 kHz, reveals that only the holmium complex **9** shows a frequency-dependent ac response (Figure 11). A relaxation mode is clearly observed at 1.85 K around

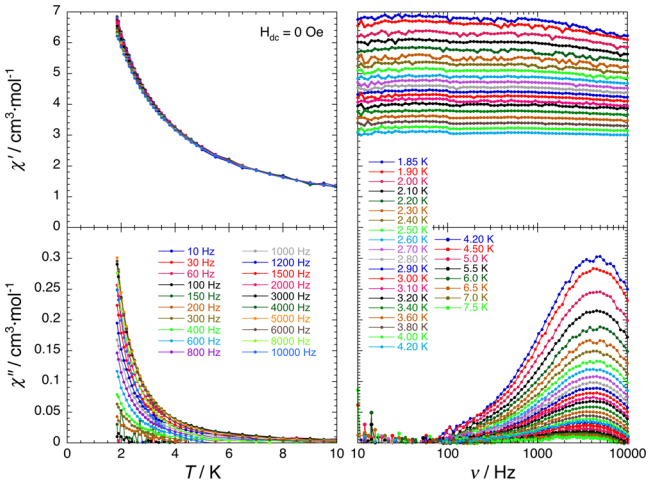

Figure 11. (left) Temperature and (right) frequency dependence of the (top) real (χ') and (bottom) imaginary (χ'') parts of the ac susceptibility, between 10 and 10 000 Hz and between 1.85 and 7.5 K, respectively, for **9** in zero dc field. Solid lines are visual guides.

4500 Hz. This mode is temperature-independent, as expected when the regime of the magnetization relaxation of an SMM is governed by quantum tunneling. Between 1.85 and 7.5 K, the characteristic relaxation time of **9** is thus constant at about 3.5 $\times$ 10^{-5} s, and no thermally activated regime of relaxation was observed experimentally.

CONCLUSIONS

The heteroditopic cyano-bisphosphonate ligand **L** provided a series of 10 Ln^{III} crystalline complexes, which crystallized in two structural types, that is, $[Ln^{III}(\mathbf{L})_3(H_2O)_2]\cdot H_2O$ (Ln = La, Pr, Nd), with eight-coordinated metal ions, and $[Ln^{III}(\mathbf{L})_3(H_2O)]\cdot 8H_2O$ (Ln = Sm, Eu, Gd, Tb, Dy, Ho, Er), containing seven-coordinated Ln^{III} ions. Although the cyano group of the ligand does not participate to the coordination of the metal, its role is clearly evidenced through the establishment of intermolecular hydrogen bonding with coordination or crystallization water molecules, thus leading to the formation of extended supramolecular architectures. The most interesting solid-state photophysical properties were observed for the Eu^{III} and Tb^{III} complexes, which show bright intense luminescence with long excited-state lifetimes of 530 and 1370 μs, respectively. Comparatively, the luminescence of the Pr^{III}, Sm^{III}, Dy^{III}, and Ho^{III} complexes is much weaker, with short lifetimes in the nanosecond and microsecond regime. The magnetic properties are in agreement with isolated Ln^{III} ions in the solid state, and they show the usual temperature-dependent behavior with the gradual depopulation of the Stark levels, except for the Gd^{III} analogue. Interestingly, the Ho^{III} complex shows a frequency-dependent ac response, with a relaxation mode observed at 1.85 K around 4500 Hz. This mode is temperature-independent, which is typical of an SMM with the magnetization relaxation governed by quantum tunneling.

This first series of Ln^{III} complexes based on the ditopical ligand **L** clearly demonstrates the interest of such ligand. Potentially, the CN group can also engage in coordination with a different metal center to provide extended luminescent and/or magnetic networks. Moreover, the attachment of unsaturated or chromophor units to the ligand could favor the antenna effect and thus the enhancement of the emissive properties of the Ln^{III}-containing complexes.

EXPERIMENTAL SECTION

General. Reactions were carried out under normal atmosphere and with solvents of commercial purity. The IR spectra were recorded on KBr pellets with a Bruker TENSOR 37 spectrophotometer in the 4000–400 cm^{-1} range.

Syntheses. Except when specifically mentioned, all the chemicals were purchased from commercial sources and were used as received. The bphosCN ligand **L** was obtained as already reported.[17,18] All the complexes were synthesized by the same general procedure: to a solution of **L** (0.05 mmol) in 20 mL of ethanol (EtOH) were added 20 mL of EtOH solution of $Ln(NO_3)_3\cdot xH_2O$ (0.05 mmol). The resulting solutions were stirred for about 1.5 h and then filtered. The slow evaporation of the filtrate at room temperature yielded unstable crystals after several days. The desired crystals were obtained after recrystallization from water.

$[La^{III}(L)_3(H_2O)_2]\cdot H_2O$ ***(1)***. Selected IR bands (KBr, cm^{-1}): 3481(OH), 2974, 2891(CH), 2181(CN), 1048(P–O), 634, 568, 476. Anal. Calcd. for $C_{36}H_{66}LaN_3O_{21}P_6$: C, 35.98; H, 5.53; N, 3.49. Found C, 35.78; H, 5.21; N, 3.75%.

$[Pr^{III}(L)_3(H_2O)_2]\cdot H_2O$ ***(2)***. Selected IR bands (KBr, cm^{-1}): 3413(OH), 2971, 2886(CH), 2180(CN), 1050(P–O), 634, 570, 479. Anal. Calcd. for $C_{36}H_{66}PrN_3O_{21}P_6$: C, 35.92; H, 5.52; N, 3.49. Found C, 40.10; H, 5.31; N, 3.65%.

$[Nd^{III}(L)_3(H_2O)_2]\cdot H_2O$ ***(3)***. Selected IR bands (KBr, cm^{-1}): 3397(OH), 2971, 2886(CH), 2180(CN), 1049(P–O), 634, 570, 478. Anal. Calcd. for $C_{36}H_{66}NdN_3O_{21}P_6$: C, 35.82; H, 5.51; N, 3.48. Found C, 35.49; H, 5.65; N, 3.65%.

$[Sm^{III}(L)_3(H_2O)]\cdot 8H_2O$ ***(4)***. Selected IR bands (KBr, cm^{-1}): 3402(OH), 2973, 2886(CH), 2180(CN), 1049(P–O), 634, 570, 479. Anal. Calcd. for $C_{36}H_{76}N_3O_{27}P_6Sm$: C, 32.77; H, 5.80; N, 3.18. Found C, 32.64; H, 5.61; N, 3.15%.

$[Eu^{III}(L)_3(H_2O)]\cdot 8H_2O$ ***(5)***. Selected IR bands (KBr, cm^{-1}): 3380(OH), 2974, 2887(CH), 2181(CN), 1048(P–O), 639, 570, 478. Anal. Calcd. for $C_{36}H_{76}N_3O_{27}P_6Eu$: C, 32.73; H, 5.79; N, 3.18. Found C, 32.59; H, 5.96; N, 3.28%.

$[Gd^{III}(L)_3(H_2O)]\cdot 8H_2O$ ***(6)***. Selected IR bands (KBr, cm^{-1}): 3420(OH), 2975(CH), 2186(CN), 1048(P–O), 635, 570, 480. Anal. Calcd. for $C_{36}H_{76}N_3O_{27}P_6Gd$: C, 32.60; H, 5.77; N, 3.16. Found C, 39.67; H, 5.21; N, 3.75%.

$[Tb^{III}(L)_3(H_2O)]\cdot 8H_2O$ ***(7)***. Selected IR bands (KBr, cm^{-1}): 3500(OH), 2977, 2891(CH), 2179(CN), 1049(P–O), 665, 569, 476. Anal. Calcd. for $C_{36}H_{76}N_3O_{27}P_6Tb$: C, 32.56; H, 5.59; N, 3.88. Found C, 32.68; H, 5.46; N, 3.95%.

$[Dy^{III}(L)_3(H_2O)]\cdot 8H_2O$ ***(8)***. Selected IR bands (KBr, cm^{-1}): 3429(OH), 2975, 2891 (CH), 2186(CN), 1048(P–O), 636, 571, 480. Anal. Calcd. for $C_{36}H_{76}N_3O_{27}P_6Dy$: C, 32.47; H, 5.75; N, 3.15. Found C, 32.69; H, 5.86; N, 3.49%.

dx.doi.org/10.1021/ic403104y | Inorg. Chem. 2014, 53, 2708–2717

Table 4. Crystallographic Data, Details of Data Collection, and Structure Refinement Parameters

compound	1	2	3	4	5
chemical formula	$C_{36}H_{60}LaN_3O_{21}P_6$	$C_{36}H_{60}N_3O_{21}P_6Pr$	$C_{36}H_{60}N_3NdO_{21}P_6$	$C_{36}H_{60}N_3O_{27}P_6Sm$	$C_{36}H_{60}EuN_3O_{27}P_6$
formula weight (g/mol)	1195.60	1197.60	1200.93	1303.04	1304.65
crystal system	orthorhombic	orthorhombic	orthorhombic	monoclinic	monoclinic
space group	$P2_12_12_1$	$P2_12_12_1$	$P2_12_12_1$	Pn	Pn
a (Å)	12.172(2)	12.1705(8)	12.1304(8)	11.1318(7)	11.1476(8)
b (Å)	16.5748(10)	16.5077(12)	16.5237(10)	11.8742(9)	11.8848(8)
c (Å)	26.694(3)	26.6601(17)	26.6343(18)	22.8997(14)	22.9395(17)
α (deg)	90.00	90.00	90.00	90.00	90.00
β (deg)	90.00	90.00	90.00	91.818(8)	91.810(9)
γ (deg)	90.00	90.00	90.00	90.00	90.00
volume (Å^3), Z	5385.5(12), 4	5356.2(6), 4	5338.6(6), 4	3025.4(4), 2	3037.7(4), 2
temperature (K)	293(2)	293(2)	293(2)	293(2)	293(2)
calculated density (Mg m^{-3})	1.475	1.485	1.494	1.430	1.426
Flack parameter	0.006(7)	−0.018(6)	−0.019(7)	−0.026(6)	0.015(7)
absorption coefficient (mm^{-1})	1.044	1.161	1.225	1.206	1.267
final R^a indices [$I > 2\sigma(I)$]	R_1 = 0.0335	R_1 = 0.0264	R_1 = 0.0321	R_1 = 0.0330	R_1 = 0.0387
	wR_2 = 0.0695	wR_2 = 0.0653	wR_2 = 0.0797	wR_2 = 0.0820	wR_2 = 0.0868
R indices (all data)	R_1 = 0.0488	R_1 = 0.0295	R_1 = 0.0352	R_1 = 0.0377	R_1 = 0.0609
	wR_2 = 0.0747	wR_2 = 0.0663	wR_2 = 0.0809	wR_2 = 0.0840	wR_2 = 0.0976
goodness-of-fit on F^2	1.066	1.019	1.013	0.976	0.927
$\Delta\rho_{min}$ and $\Delta\rho_{max}$ (e Å^{-3})	0.355 and −0.515	0.431 and −0.324	0.584 and −0.332	0.647 and −0.631	0.604 and −0.483
compound	6	7	8	9	10
chemical formula	$C_{36}H_{60}GdN_3O_{27}P_6$	$C_{36}H_{60}N_3O_{27}P_6Tb$	$C_{36}H_{60}DyN_3O_{27}P_6$	$C_{36}H_{60}HoN_3O_{27}P_6$	$C_{36}H_{60}ErN_3O_{27}P_6$
formula weight (g/mol)	1309.94	1311.61	1315.19	1317.62	1319.95
crystal system	monoclinic	monoclinic	monoclinic	monoclinic	monoclinic
space group	Pn	Pn	Pn	Pn	Pn
a (Å)	11.1440(4)	11.1296(9)	11.1300(8)	11.1386(8)	11.1375(8)
b (Å)	11.8806(9)	11.8385(7)	11.8510(10)	11.8158(9)	11.7850(8)
c (Å)	22.934(2)	22.875(2)	22.8564(18)	22.8715(17)	22.8365(17)
α (deg)	90.00	90.00	90.00	90.00	90.00
β (deg)	91.716(6)	91.622(11)	91.699(9)	91.579(9)	91.817(9)
γ (deg)	90.00	90.00	90.00	90.00	90.00
volume (Å^3), Z	3035.1(4), 2	3012.7(4), 2	3013.5(4), 2	3009.0(4), 2	2995.9(4), 2
temperature (K)	293(2)	293(2)	293(2)	293(2)	293(2)
calculated density (Mg m^{-3})	1.433	1.446	1.449	1.454	1.463
Flack parameter	0.132(6)	0.012(7)	−0.008(6)	−0.015(5)	0.542(13)
absorption coefficient (mm^{-1})	1.328	1.411	1.477	1.552	1.639
final R^a indices [$I > 2\sigma(I)$]	R_1 = 0.0397	R_1 = 0.0361	R_1 = 0.0348	R_1 = 0.0282	R_1 = 0.0487
	wR_2 = 0.0618	wR_2 = 0.0514	wR_2 = 0.0742	wR_2 = 0.0594	wR_2 = 0.0963
R indices (all data)	R_1 = 0.0649	R_1 = 0.0579	R_1 = 0.0424	R_1 = 0.0334	R_1 = 0.1437
	wR_2 = 0.0671	wR_2 = 0.0554	wR_2 = 0.0775	wR_2 = 0.0602	wR_2 = 0.1299
goodness-of-fit on F^2	0.999	0.844	0.996	1.173	0.761
$\Delta\rho_{min}$ and $\Delta\rho_{max}$ (e Å^{-3})	0.653 and −0.393	0.855 and −0.488	1.027 and −1.072	0.726 and −0.675	0.912 and −2.364

$^a R(F_o) = \sum||F_o|-|F_c||/\sum|F_o|$; $R_w(F_o^2) = [\sum[w(F_o^2-F_c^2)^2]/\sum[w(F_o^2)^2]]^{1/2}$

*$[Ho^{III}(L)_3(H_2O)]\cdot 8H_2O$ (**9**).* Selected IR bands (KBr, cm^{-1}): 3371(OH), 2977(CH), 2892(CH), 2187(CN), 1047(P−O), 635, 570, 480. Anal. Calcd. for $C_{36}H_{76}N_3O_{27}P_6Ho$: C, 32.41; H, 5.74; N, 3.15. Found C, 32.58; H, 5.66; N, 3.33%.

*$[Er^{III}(L)_3(H_2O)]\cdot 8H_2O$ (**10**).* Selected IR bands (KBr, cm^{-1}): 3358(OH), 2974(CH), 2887(CH), 2181(CN), 1048(P−O), 634, 570, 478. Anal. Calcd. for $C_{36}H_{76}N_3O_{27}P_6Er$: C, 32.36; H, 5.73; N, 3.14. Found C, 32.45; H, 5.67; N, 3.49%.

X-ray Structure Determinations. Details about data collection and solution refinement are given in Table 4. X-ray diffraction measurements were performed on a Bruker Kappa CCD diffractometer for complexes **1**, **5**, and **6** and on a STOE IPDS I diffractometer for complexes **2**−**4** and **7**−**10**, both operating with a Mo Kα (λ = 0.71073 Å) X-ray tube with a graphite monochromator. The structures were solved (SHELXS-97) by direct methods and refined (SHELXL-97) by full-matrix least-squares procedures on F^2.[28] All non-H atoms of the donor molecules were refined anisotropically, and hydrogen atoms were introduced at calculated positions (riding model), included in structure factor calculations but not refined. The H atoms for the water molecules were not located in the Fourier maps and were not included in chemical formula of the cifs files. Crystallographic data for the structures have been deposited in the Cambridge Crystallographic Data Centre (see Supporting Information).

Photophysical Measurements. The photoluminescence (PL) measurements were carried out using a Fluoromax 4 spectrofluorometer (Horiba) operated in both the fluorescence and the phosphorescence modes. The repetition rate of the xenon flash lamp was 25 Hz, the integration window varied between 0.3 and 3 s, and up to 100 flashes were accumulated per data point. The slits bandpasses were varied from 0.001 to 29 nm in excitation as well as emission. PL decays were measured by using the "decay by delay" feature of the

dx.doi.org/10.1021/ic403104y | Inorg. Chem. 2014, 53, 2708−2717

phosphorescence mode. The laser-excited time-resolved emission spectra were recorded at room temperature using a wavelength tunable NT340 Series EKSPLA OPO (Optical Parametric Oscillator) operated at 20 Hz as excitation light source and an intensified Charge-Coupled Device (CCD) camera (Andor Technology) coupled to a spectrograph (Shamrock 303i, Andor) as detection system. The time-resolved PL spectra were collected using the boxcar technique. The emission was detected in the spectral range of $400 < \lambda_{em} < 800$ nm, with a spectral resolution of 0.3 nm. The PL decays were analyzed by fitting with a multiexponential function $f(t)$, using the commercial software (OriginPro 8): $f(t) = \sum A_i \exp(-t/\tau_i) + B$, where A_i is the decay amplitude, B is a constant (the baseline offset), and τ_i is the time constant of the decay i.

Magnetic Measurements. The magnetic measurements were performed using Quantum Design MPMS-XL SQUID magnetometers and a Quantum Design physical property measurement system (PPMS-9). The measurements were performed on polycrystalline samples introduced in polyethylene bags (3 × 0.5 × 0.02 cm). The dc measurements were conducted from 300 to 1.8 K and between −70 and 70 kOe applied dc fields. An M versus H measurement was performed at 100 K to confirm the absence of ferromagnetic impurities. The field dependence of the magnetization was measured between 1.83 and 8 K with a dc magnetic field between 0 and 7 T. The ac susceptibility experiments were performed at various frequencies ranging from 1 to 10 000 Hz, with ac field amplitudes of 1−5 Oe, with or wihout the application of a static (dc) field. Experimental data were corrected for diamagnetic contributions from the sample holder and the sample.

■ ASSOCIATED CONTENT

Ⓢ Supporting Information

X-ray crystallographic file in CIF format, photophysical and magnetic measurements. This material is available free of charge via the Internet at http://pubs.acs.org. Crystallographic data for the structures have been deposited in the Cambridge Crystallographic Data Centre, deposition numbers CCDC 977936 (**1**), CCDC 977937 (**2**), CCDC 977938 (**3**), CCDC 977939 (**4**), CCDC 977940 (**5**), CCDC 977941 (**6**), CCDC 977942 (**7**), CCDC 977943 (**8**), CCDC 977944 (**9**), CCDC 977945 (**10**). These data can be obtained free of charge from The Cambridge Crystallographic Data Centre via www.ccdc.cam.ac.uk/data_request/cif.

■ AUTHOR INFORMATION

Corresponding Author

*E-mail: narcis.avarvari@univ-angers.fr. Fax: (+33)02 41 73 54 05. Tel: (+33)02 41 73 50 84.

Notes

The authors declare no competing financial interest.

■ ACKNOWLEDGMENTS

This Work was supported by the CNRS, the University of Angers, the University of Bordeaux, the Régions Pays de la Loire (grant to D.B.) and Aquitaine, and the National Agency for Research (ANR) (ANR Inter, ANR-12-IS07-0004-04, CREMM project). Financial support from a Brancusi 2009−2010 (PHC 19613XM) project is gratefully acknowledged. This Work was also supported by a grant of the Romanian National Authority for Scientific Research, CNCS−UEFISCDI, Project Number PN-II-RU-TE-2012-3-0422. C.T. acknowledges partial support from the COST program Action CM1006 "EUFEN: European F-Element Network."

■ DEDICATION

**Dedicated to Prof. Miguel Julve on the occasion of his 60th anniversary.

■ REFERENCES

(1) (a) Mackay, L. G.; Anderson, H. L.; Sanders, J. K. M. *J. Chem. Soc., Perkin Trans. 1* **1995**, 2269−2273. (b) Turner, S. S.; Collison, D.; Mabbs, F. E.; Halliwell, M. *J. Chem. Soc., Dalton Trans.* **1997**, 1117−1118. (c) Vreshch, V. D.; Chernega, A. N.; Howard, J. A. K.; Sieler, J.; Domasevitch, K. V. *Dalton Trans.* **2003**, *32*, 1707−1711. (d) Chen, B.; Fronczek, F. R.; Maverick, A. W. *Inorg. Chem.* **2004**, *43*, 8209−8211. (e) Vreshch, V. D.; Lysenko, A. B.; Chernega, A. N.; Howard, J. A. K.; Krautscheid, H.; Sieler, J.; Domasevitch, K. V. *Dalton Trans.* **2004**, *33*, 2899−2903. (f) Zhang, Y.; Chen, B.; Fronczek, F. R.; Maverick, A. W. *Inorg. Chem.* **2008**, *47*, 4433−4435.

(2) Silvernail, C. M.; Yap, G.; Sommer, R. D.; Rheingold, A. L.; Dayand, V. W.; Belot, J. A. *Polyhedron* **2001**, *20*, 3113−3117.

(3) (a) Angelova, O.; Petrov, G.; Macicek, J. *Acta Crystallogr., Sect. C: Cryst. Struct. Commun.* **1989**, *45*, 710−713. (b) Angelova, O.; Macicek, J.; Atanasov, M.; Petrov, G. *Inorg. Chem.* **1991**, *30*, 1943−1949.

(4) Voutsas, G.; Tzavellas, L. C.; Tsiamis, C. *Struct. Chem.* **1999**, *10*, 53−57.

(5) Tsiamis, C.; Hatzidimitriou, A. G.; Tzavellas, L. C. *Inorg. Chem.* **1998**, *37*, 2903−2909.

(6) Burrows, A. D.; Cassar, K.; Mahon, M. F.; Warren, J. E. *Dalton Trans.* **2007**, *36*, 2499−2509.

(7) Merkens, C.; Becker, N.; Lamberts, K.; Englert, U. *Dalton Trans.* **2012**, *41*, 8594−8599.

(8) Kondracka, M.; Englert, U. *Inorg. Chem.* **2008**, *47*, 10246−10257.

(9) (a) Pogozhev, D.; Baudron, S. A.; Hosseini, M. W. *Inorg. Chem.* **2010**, *49*, 331−338. (b) Kilduff, B.; Pogozhev, D.; Baudron, S. A.; M. W. Hosseini, M. W. *Inorg. Chem.* **2010**, *49*, 11231−11239.

(10) Della Pia, E. A.; Døssing, A.; Kilså, K. *Inorg. Chim. Acta* **2013**, *395*, 72−76.

(11) Merkens, C.; Englert, U. *Dalton Trans.* **2012**, *41*, 4664−4673.

(12) (a) Parker, D. *Coord. Chem. Rev.* **2000**, *205*, 109−130. (b) De Silva, A. P.; Fox, D. B.; Huxley, A. J. M.; Moody, T. S. *Coord. Chem. Rev.* **2000**, *205*, 41−57. (c) de Bettencourt-Dias, A. *Dalton Trans.* **2007**, *36*, 2229−2241. (d) Bünzli, J.-C. G. *Chem. Lett.* **2009**, *38*, 104−109.

(13) Eliseeva, S. V.; Bünzli, J-C. G. *Chem. Soc. Rev.* **2010**, *39*, 189−227.

(14) polynuclear complexes: (a) Tang, J.; Hewitt, I.; Madhu, N. T.; Chastanet, G.; Wernsdorfer, W.; Anson, C. E.; Benelli, C.; Sessoli, R.; Powell, A. K. *Angew. Chem., Int. Ed.* **2006**, *45*, 1729−1733. (b) Anwar, M. U.; Thompson, L. K.; Dawe, L. N.; Habib, F.; Murugesu, M. *Chem. Commun.* **2012**, *48*, 4576−4578. (c) Vallejo, J.; Cano, J.; Castro, I.; Julve, M.; Lloret, F.; Fabelo, O.; Cañadillas-Delgado, L.; Pardo, E. *Chem. Commun.* **2012**, *48*, 7726−7728. (d) Gao, F.; Li, Y.-Y.; Liu, C.-M.; Lia, Y.-Z.; Zuo, J.-L. *Dalton Trans.* **2013**, *42*, 11043−11046. (e) Kan, J.; Wang, H.; Sun, W.; Cao, W.; Tao, J.; Jiang, J. *Inorg. Chem.* **2013**, *52*, 8505−8510. (f) Sun, W.-B.; Han, B.-L.; Lin, P.-H.; Li, H.-F.; Chen, P.; Tian, Y.-M.; Murugesu, M.; Yan, P.-F. *Dalton Trans.* **2013**, *42*, 13397−13403. (g) Habib, F.; Murugesu, M. *Chem. Soc. Rev.* **2013**, *42*, 3278−3288. (h) Zhang, P.; Guo, Y.-N.; Tang, J. *Coord. Chem. Rev.* **2013**, *257*, 1728−1763. (i) Woodruff, D. N.; Winpenny, R. E. P.; Layfield, R. A. *Chem. Rev.* **2013**, *113*, 5110−5148. (j) Blagg, R. J.; Ungur, L.; Tuna, F.; Speak, J.; Comar, P.; Collison, D.; Wernsdorfer, W.; McInnes, E. J. L.; Chibotaru, L. F.; Winpenny, R. E. P. *Nature Chem.* **2013**, *5*, 673−678.

(15) Mononuclear complexes: (a) Ishikawa, N.; Sugita, M.; Ishikawa, T.; Koshihara, S.; Kaizu, Y. *J. Am. Chem. Soc.* **2003**, *125*, 8694−8695. (b) Ishikawa, N.; Sugita, M.; Wernsdorfer, W. *Angew. Chem., Int. Ed.* **2005**, *44*, 2931−2935. (c) Rinehart, J. D.; Long, J. R. *Chem. Sci.* **2011**, *2*, 2078−2085. (d) Jiang, S.-D.; Liu, S.-S.; Zhou, L.-N.; Wang, B.-W.; Wang, Z.-M.; Gao, S. *Inorg. Chem.* **2012**, *51*, 3079−3087. (e) Gonidec, M.; Amabilino, D. B.; Veciana, J. *Dalton Trans.* **2012**, *41*, 13632−13639. (f) Luzon, J.; Sessoli, R. *Dalton Trans.* **2012**, *41*, 13556−13567.

(g) Cucinotta, G.; Perfetti, M.; Luzon, J.; Etienne, M.; Car, P.-E.; Caneschi, A.; Calvez, G.; Bernot, K.; Sessoli, R. *Angew. Chem., Int. Ed.* **2012**, *51*, 1606−1610. (h) Wang, Y.-L.; Ma, Y.; Yang, X.; Tang, J.; Cheng, P.; Wang, Q.-L.; Li, L.-C.; Liao, D.-Z. *Inorg. Chem.* **2013**, *52*, 7380−7386. (i) Pointillart, F.; Le Guennic, B.; Cauchy, T.; Golhen, S.; Cador, O.; Maury, O.; Ouahab, L. *Inorg. Chem.* **2013**, *52*, 5978−5990. (j) Gonidec, M.; Krivokapic, I.; Vidal-Gancedo, J.; Davies, E. S.; McMaster, J.; Gorun, S. M.; Veciana, J. *Inorg. Chem.* **2013**, *52*, 4464−4471. (k) Chilton, N. F.; Langley, S. K.; Moubaraki, B.; Soncini, A.; Batten, S. R.; Murray, K. S. *Chem. Sci.* **2013**, *4*, 1719−1730.

(16) (a) Bogani, L.; Sangregorio, C.; Sessoli, R.; Gatteschi, D. *Angew. Chem., Int. Ed.* **2005**, *44*, 5817−5821. (b) Bernot, K.; Bogani, L.; Caneschi, A.; Gatteschi, D.; Sessoli, R. *J. Am. Chem. Soc.* **2006**, *128*, 7947−7956.

(17) Maxim, C.; Branzea, D.; Allain, M.; Andruh, M.; Clérac, R.; Iorga, B. I.; Avarvari, N. *CrystEngComm* **2012**, *14*, 3096−3102.

(18) Iorga, B.; Ricard, L.; Savignac, P. *J. Chem. Soc., Perkin Trans. 1* **2000**, *29*, 3311−3316.

(19) Blanton, W. B.; Gordon-Wylie, S. W.; Clark, G. R.; Jordan, K. D.; Wood, J. T.; Geiser, U.; Collins, T. J. *J. Am. Chem. Soc.* **1999**, *121*, 3551−3552.

(20) (a) Ene, C. D.; Madalan, A. M.; Maxim, C.; Jurca, B.; Avarvari, N.; Andruh, M. *J. Am. Chem. Soc.* **2009**, *131*, 4586−4587. (b) Maxim, C.; Sorace, L.; Khuntia, P.; Madalan, A. M.; Kravtsov, V.; Lascialfari, L.; Caneschi, A.; Journaux, Y.; Andruh, M. *Dalton Trans.* **2010**, *39*, 4838−4847.

(21) Tiseanu, C.; Cojocaru, B.; Avram, D.; Parvulescu, V. I.; Vela-Gonzalez, A. V.; Sanchez-Dominguez, M. *J. Phys. D: Appl. Phys.* **2013**, *46*, 275302−1−8.

(22) (a) Pasatoiu, T.; Madalan, A.; Kumke, M.; Tiseanu, C.; Andruh, M. *Inorg. Chem.* **2010**, *49*, 2310−2315. (b) Pasatoiu, T.; Tiseanu, C.; Madalan, A.; Jurca, B.; Duhayon, C.; Sutter, J.-P.; Andruh, M. *Inorg. Chem.* **2011**, *50*, 5879−5889.

(23) Blasse, G.; Brill, A.; Nieuwpoort, W. C. *J. Phys. Chem. Solids* **1966**, *27*, 1587−1592.

(24) Dorenbos, P. *J. Lumin.* **2000**, *91*, 155−176.

(25) Pasatoiu, T.; Madalan, A.; Zamfirescu, M.; Tiseanu, C.; Andruh, M. *Phys. Chem. Chem. Phys.* **2012**, *32*, 11448−11456.

(26) (a) Kahn, O. *Molecular Magnetism;* Wiley-VCH: Weinheim, Germany, 1993. (b) Benelli, C.; Gatteschi, D. *Chem. Rev.* **2002**, *102*, 2369−2388.

(27) (a) Sutter, J.-P.; Kahn, M. L. In *Magnetism: Molecules to Materials;* Miller, J.S.; Drillon, M., Eds.; Wiley-VCH: Weinheim, Germany, 2005; Vol. *5*, pp 161−188. (b) Sutter, J.-P.; Kahn, M. L.; Kahn, O. *Adv. Mater.* **1999**, *11*, 863−865. (c) Kahn, M. L.; Sutter, J.-P.; Golhen, S.; Guionneau, P.; Ouahab, L.; Kahn, O.; Chasseau, D. *J. Am. Chem. Soc.* **2000**, *122*, 3413−3421. (d) Sutter, J.-P.; Kahn, M. L.; Mörtl, K. P.; Ballou, R.; Porcher, P. *Polyhedron* **2001**, *20*, 1593−1597. (e) Kahn, M. L.; Ballou, R.; Porcher, P.; Kahn, O.; Sutter, J.-P. *Chem.—Eur. J.* **2002**, *8*, 525−531.

(28) Sheldrick, G. M. *Programs for the Refinement of Crystal Structures;* University of Göttingen: Göttingen, Germany, 1996.

dx.doi.org/10.1021/ic403104y | *Inorg. Chem.* 2014, 53, 2708−2717